Available online at www.sciencedirect.com
SCIENCE DIRECT®
Inorganica Chimica Acta 359 (2006) 1071–1080
Inorganica Chimica Acta
www.elsevier.com/locate/ica

Synthesis, structures and electrochemical properties of amino-derivatives of diiron azadithiolates as active site models of Fe-only hydrogenase

Weiming Gao [a], Jianhui Liu [a,*], Chengbing Ma [b], Linhong Weng [c], Kun Jin [a], Changneng Chen [b], Björn Åkermark [d], Licheng Sun [a,e,*]

[a] State Key Laboratory of Fine Chemicals, Dalian University of Technology, Zhongshan Road 158-40, Dalian 116012, PR China
[b] State Key Laboratory of Structural Chemistry, Fujian Institute of Research on the Structure of Matter, Fuzhou 350002, PR China
[c] Chemistry Department, Fudan University, Handan Road 220, Shanghai 200433, PR China
[d] Department of Organic Chemistry, Arrhenius Laboratory, Stockholm University, 10691 Stockholm, Sweden
[e] KTH Chemistry, Organic Chemistry, Royal Institute of Technology, 10044 Stockholm, Sweden

Received 27 June 2005; received in revised form 16 October 2005; accepted 26 October 2005
Available online 18 January 2006

Abstract

The preparation and characterization of two novel amino-incorporated sulfur-bridged dinuclear iron (I) complexes of the type [NR(μ-$SCH_2)_2$]$Fe_2(CO)_6$, one being amino protected [$N(CH_2CH_2NHTs)(\mu$-$SCH_2)_2$]$Fe_2(CO)_6$ (**8**) and the other [(μ- $SCH_2)_2Fe_2(CO)_6NCH_2CH_2N$ (μ-$SCH_2)_2$]$Fe_2(CO)_6$ (**9**) are described. These two complexes are readily prepared in a S_N2 manner between double lithium anion and bis(chloromethyl) amine derivatives. The structures of **8** and **9** were characterized by IR, ^1H, ^{13}C NMR, MS and HRMS spectra and further determined by X-ray analyses. Protonation of complex **8** gave the mono *N*-protonated product, while for **9** the protonation occurred in both of the N atoms. The redox properties were evaluated by cyclic voltammograms. It was shown that these two complexes can catalyze electrochemical reduction of proton to molecular hydrogen.

Keywords: Bioinorganic chemistry; Catalysis; Hydrogen production; Iron–sulfur complex

1. Introduction

Since the first crystal structure of the Fe-only hydrogenase was reported in 1998 [1], the chemistry of iron–sulfur complexes has found significant applications in close mimics to the active site of this natural system [2–5]. The X-ray crystallographic studies revealed that the active site of Fe-only hydrogenase, also called H-cluster, consisted of a 4Fe4S cubane structure bridged with cysteine-S to a 2Fe2S subunit [1,6]. PDT (propanedithiolate, $–SCH_2CH_2CH_2S–$) and ADT (azadithiolate, $–SCH_2NHCH_2S–$) had been proposed as two types of bridging dithiolate ligands based on the central atom (carbon or nitrogen) [7]. Very recent crystallographic studies with higher resolution [7], together with DFT calculations [8], suggested that ADT or the *N*-substituted equivalent (Fig. 1(a)) was the likely structure subunit. Nevertheless, the sulfur bridged binuclear complexes containing either PDT or ADT features the model structural aspects of the Fe-only hydrogenase. The architecture shown in Fig. 1(b) was the leading model for the active site of hydrogenase, based on which much work has been performed including the structure modifications by ligand exchange and bridge variation [9–18]. The incorporation of suitably functionalized moieties at defined sites facilitates the study to mimic the behavior of metal–sulfur

* Corresponding authors. Tel./fax: +86 411 8370 2185.
E-mail addresses: liujh@dlut.edu.cn (J. Liu), lichengs@kth.se (L. Sun).

0020-1693/$ - see front matter © 2005 Elsevier B.V. All rights reserved.
doi:10.1016/j.ica.2005.10.053

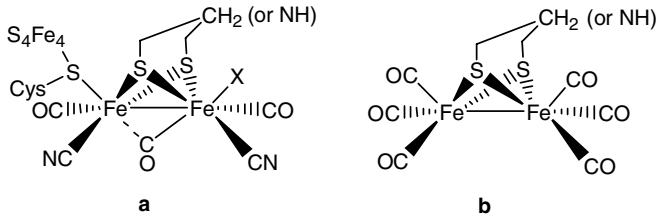

Fig. 1. The active site of Fe-only hydrogenase (a) and its leading model structure (b).

sites in hydrogenase. For the ADT series, *N*-alkyl, *N*-benzyl and *N*-substituted phenyl analogues have been reported [19,20]. Among them the *N*-benzyl substituted Fe_2S_2 system, which had only one carbon atom between the N atom and the phenyl group, shows better behavior for catalyzing protons to produce hydrogen [20]. Such a conformation forces the benzyl moiety into a pseudo-equatorial position and keeps the N lone-pair pointing towards an iron nucleus. This prompted us to design a new kind of ADT complex with $NH_2CH_2CH_2$– as the N substituent featured with a terminal free amino group connected to the substituent by a two carbon unit. Through this free amino group, a photosensitizer could potentially be attached to the active site model of hydrogenase [21,22]. The present work will report the synthesis of Ts protected amino derivatives **8**, and the formation of the expected dimer **9** as well as their structure characterizations. Both compounds are found to be good catalysts for electrochemical reduction of protons to molecular hydrogen.

2. Experimental

2.1. Reagents and instruments

All reactions and operations related to organometallic complexes were carried out under a dry, oxygen-free nitrogen atmosphere with standard Schlenk techniques. All solvents were dried and distilled prior to use according to the standard methods. Commercially available chemicals, including perchloric acid (only used for the UV–Vis measurement), paraformaldehyde, *p*-tosyl chloride, ethylene diamine and $Fe(CO)_5$ were used without further purification. The reagents $LiEt_3BH$ and triflic acid were purchased from Aldrich. $(\mu\text{-LiS})_2Fe_2(CO)_6$ (**6**) and $(\mu\text{-HS})_2Fe_2(CO)_6$ (**7**) were prepared according to the literature procedures [23] and they were used in situ immediately for the further reaction.

Infrared spectra were recorded on a JASCO FT/IR 430 spectrophotometer. ^1H and ^{13}C NMR were collected on a Varian INOVA 400 NMR spectrometer. Mass spectra were recorded on an HP1100 MSD instrument. HRMS were recorded on a HPLC-Q-Tof MS (Micro) system. Gas chromatography was performed with a GC7890 instrument under isothermal conditions with nitrogen as a carrier gas and a thermal conductivity detector (TCD).

2.2. Crystal structure determination

Diffraction data of compound **8** and **9** were collected on a Siemens Smart CCD diffractometer equipped with graphite monochromated Mo Kα radiation ($\lambda = 0.71073$ Å). The structures were solved by direct methods and subsequent difference Fourier syntheses, and refined by the full-matrix least squares on (F^2) by using the SHELXL-97 program. The hydrogen atoms were placed in calculated positions and were held riding on their parent non-hydrogen atoms during the subsequent refinement calculations. All non-hydrogen atoms were refined with anisotropic thermal displacement parameters.

2.3. Procedures

2.3.1. Compound 2

A solution of *p*-tosyl chloride (20 g, 0.1 mol) in benzene (50 mL) was added to ethylenediamine (**1**) (67 mL, 1.0 mol) and the mixture was stirred for 4.5 h at 40 °C. Then benzene was removed on a rotary evaporator. The crude product was purified by crystallization in water to give compound **2** as a white solid (16.8 g, 79%). ^1H NMR ($CDCl_3$): δ 2.43 (s, 3H), 2.81 (t, $J = 11.2$ Hz, 2H), 2.97 (t, $J = 11.2$ Hz, 2H), 7.31 (d, $J = 8.4$ Hz, 2H), 7.75 (d, $J = 8.4$ Hz, 2H). MS (API-ES): m/z 215 $[M + H]^+$.

2.3.2. Complex 8

Method A: A mixture of compound **2** (2.14 g, 10 mmol) and paraformaldehyde (0.6 g, 20 mmol) in THF (40 mL) was stirred for 4 h. It was cooled to 0 °C and then freshly distilled $SOCl_2$ (2.84 mL, 40 mmol) was added dropwise. After further stirring for 1.5 h, THF and unreacted $SOCl_2$ were removed under vacuum, and the residue was added to $(LiS)_2Fe_2(CO)_6$ (**6**) (1 mmol) in THF (40 mL) at −78 °C. The reaction mixture was stirred for 1 h at this temperature and then warmed to rt. After filtration, the solvent was removed by evaporation on a rotary evaporator. The crude product was purified by column chromatography with CH_2Cl_2/hexane (1/1 v/v) as eluent to give **8** (288 mg, 49%) as a red solid. IR (KBr): ν(CO) 2073, 2029, 1992 cm^{-1}; ^1H NMR ($CDCl_3$): δ (ppm) 2.44 (s, 3H), 2.79 (s, 2H), 2.86 (s, 2H), 3.42 (s, 4H), 7.32 (d, $J = 6.4$ Hz, 2H), 7.70 (d, $J = 6.4$ Hz, 2H). ^{13}C NMR δ (ppm) 21.73, 29.87, 40.92, 52.74, 56.05, 127.17, 130.05, 136.79, 144.03, 207.75. MS (API-ES): m/z: 619.1 $[M + Cl]^-$. HRMS (ESI): m/z $[M - H]^-$ calcd for 582.8690, found: 582.8705. Elemental analysis for $C_{17}H_{16}Fe_2N_2O_8S_3$, Calc. C, 34.95; H, 2.76; N, 4.80. Found: C, 35.44; H, 2.56; N, 4.82%.

Method B: The mixture of complex **2** (2.14 g, 10 mmol) and paraformaldehyde (0.6 g, 20 mmol) in THF (40 mL) was stirred for 4 h. Then it was cooled to 0 °C and the THF solution (20 mL) of $(HS)_2Fe_2(CO)_6$ (**7**) (0.5 mmol) was added. The suspension was stirred for 5 h at room temperature to afford complex **8** (146 mg, 50%).

2.3.3. Complex 9

Ethylenediamine (**1**) (0.67 mL, 10 mmol) and paraformaldehyde (0.6 g, 20 mmol) were stirred in THF (20 mL) until the solution became transparent. It was cooled to 0 °C and then freshly distilled $SOCl_2$ (2.84 mL, 40 mmol) was added dropwise to the mixture and stirred for 1 h. The solvent was removed by vacuum, then the addition of $(LiS)_2Fe_2(CO)_6$ (**6**) in the same manner as for **8** gave **9** as a dark red solid (200 mg, 50%). IR (KBr): ν(CO) 2068, 1988, 1961 cm^{-1}; ^1H NMR ($CDCl_3$): δ (ppm) 2.64 (s, 4 H), 3.54 (s, 8H) ^{13}C NMR ($CDCl_3$): δ 36.55, 53.22, 208.39. MS (API-ES): m/z 834.7 $[M + Cl]^-$. HRMS (ESI): m/z $[M + H]^+$ calcd for 800.6749, found: 800.6730. Elemental analyisis for $C_{18}H_{12}Fe_4N_2O_{12}S_4$, Calc: C, 27.03; H, 1.51; N, 3.50. Found: C, 27.19; H, 1.65; N, 3.74%.

2.3.4. Protonation of 8 and 9

A small amount of **8** (2–3 mg) was dissolved in an CD_3CN (0.5 mL) in an NMR-tube, and then two drops of triflic acid were added directly to the solution for in situ ^1H NMR analysis. The solvent was removed by vacuum to get the red solid of $\mathbf{8H}^+$ for IR analysis (KBr): ν(CO) 2091, 2039, 2027 cm^{-1}. ^1H NMR (CD_3CN): δ (ppm) 2.40 (s, 3H), 3.06 (t, $J = 5.2$ Hz, 2H), 3.22–3.29 (m, 4H), 4.29 (d, $J = 12.8$ Hz, 2H), 7.40 (d, $J = 8.0$ Hz, 2H), 7.71 (d, $J = 8.4$ Hz, 2H). Complex **9** was protonated in a similar manner to afford $\mathbf{9H}_2^{2+}$: IR (KBr): ν(CO) 2095, 2067, 2025 cm^{-1}; ^1H NMR (CD_3CN): δ (ppm) 3.21 (t, $J = 11.6$ Hz, 2H), 3.38 (s, 2H), 4.08 (d, $J = 12.0$ Hz, 2H).

2.4. Crystal data for 8 and 9

See Table 1.

Table 1
X-Ray crystallographic data for **8** and **9**

	8	**9**
Empirical formula	$C_{17}H_{16}Fe_2N_2O_8S_3$	$C_{18}H_{12}Fe_4N_2O_{12}S_4$
F_w	584.20	799.98
Crystal system	triclinic	monoclinic
Space group	$P\bar{1}$	$P2_1/n$
a (Å)	6.9917(19)	7.69140(10)
b (Å)	12.885(3)	18.4673(5)
c (Å)	13.660(4)	9.7645(3)
α (°)	94.276(4)	90.00
β (°)	104.641(4)	94.1990(10)
γ (°)	102.394(4)	90.00
V (Å^3)	1152.0(5)	1383.22(6)
Z	2	2
ρ_{calc} (g m^{-3})	1.684	1.921
T (K)	293(2)	298
μ (mm^{-1})	1.576	2.419
F(000)	592	796
Reflections measured	4845	4070
Reflections/R_{int}	3973/0.0380	2398/0.0277
Goodness-of-Fit (on F^2)	1.038	1.047
R_1 [$I > 2\sigma(I)$]	0.0764	0.0725
wR_2 (all data)	0.1985	0.2407

2.5. Electrochemistry

Acetonitrile (Aldrich, spectroscopy grade) used for performance of electrochemistry was dried with molecular sieve (4 Å) and then freshly distilled from CaH_2 under N_2. A solution of 0.05 M n-$[Bu_4N]^-[PF_6]^+$ (Fluka, electrochemical grade) in CH_3CN was used as electrolyte. Electrochemical measurements were recorded using a BAS-100W electrochemical potentiostat. The electrolyte solution was degased by bubbling with dry argon for 10 min before measurement. Cyclic voltammograms were obtained in a three-electrode cell under argon. The working electrode was a glassy carbon disc (diameter 3 mm) successively polished with 3 and 1 μm diamond pastes and sonicated in ion-free water for 10 min. The reference electrode was a non-aqueous Ag/Ag^+ electrode (1.0 mM $AgNO_3$ in CH_3CN) and the auxiliary electrode was a platinum wire.

3. Results and discussion

3.1. Synthesis and spectral characterizations

Very recently, Sun and co-workers reported an amino-functionalized model of the diiron subsite with ADT-bridge [19]. For our cases, due to the two equal free amino reactive sites in the starting ethylenediamine, we at first wished to protect one of them with the most widely used tosyl group, and then removed it after the reaction with Fe–S complex **6** or **7**. Azadithiolate **8** could be prepared through either $[(\mu\text{-}S)_2Fe_2(CO)_6]^{2-}$ or $(\mu\text{-}HS)_2Fe_2(CO)_6$ by reacting respectively with halogenated or hydroxymethylamine. Thus, ethylenediamine was mono-protected by heating with TsCl to give the mono amine **2**. This compound was allowed to react with formaldehyde to form the bis(hydromethyl) derivative **3a**. The hydroxyl groups were then replaced by chloro groups by reaction with freshly distilled $SOCl_2$ to give the bis(chloromethyl) intermediate **4a**. This was used without isolation in the next step. The sulfur-centered dianion $[(\mu\text{-}S)_2Fe_2(CO)_6]^{2-}$ (**6**) which was generated by the reaction of $(\mu\text{-}S)_2Fe_2(CO)_6$ (**5**) with $LiBEt_3H$, reacted with **4a** to afford our desired complex **8**. The dianion **6** could also be transformed to thiol complex **7** by protonation with CF_3CO_2H. Complex **8** could also be prepared directly from **7** and the diol **3a** in ca. 50% yield. Attempts to produce the free amino analogue by removing the tosyl group under a variety of conditions failed. For example, TBAF (tetrabutylammonium fluoride) gave only decomposed dark material, and HBr in phenol caused protonation of bridged amine. At this stage, diamine **1** with two free amino groups was directly reacted with $(HCHO)_n$ in a molar ratio 1:2 in the hope that the complete regio selectivity can be realized to give mono-(1,1-bischloromethyl) ethylenediamine. However this reaction took place without any regioselectivity and gave only the product **4b** after chlorization. Accordingly, the Fe_2S_2

dimer **9** was obtained by reaction of **4b** with **6**. The compounds **8** and **9** were characterized by ^{1}H and ^{13}C NMR, MS and HRMS spectra.

Due to the symmetry of both **8** and **9**, the ^{1}H NMR spectrum was simple and consistent with the X-ray structure. Both complexes exhibited broadened signals in ^{1}H NMR. The most intense peaks were observed in MS spectra at *m*/*z* 585 and 619 for **8** corresponding to $[M + H]^{+}$ (positive mode) and $[M + Cl]^{-}$ (negative mode), and at 834.7 $[M + Cl]^{-}$ for **9**. The IR spectra of **8** and **9** in KBr showed three strong CO bands in the region of 1960–2080 cm^{-1}, identical to the carbonyl stretching pattern for terminal C–O bonds. In comparison with **9**, the bands for complex **8** red shifted by 5–30 cm^{-1}. The reaction routes are outlined in Schemes 1 and 2.

3.2. Molecular structure

The crystal structures of **8** and **9** are shown in Figs. 2 and 3 respectively with atom labeling scheme, and selected bond distances and bond angles are listed in Tables 2–5. The central Fe^{I} atoms in both complexes displayed similar distorted octahedral geometry, each being coordinated by three terminal carbonyl C atoms, two bridging S atoms and the other Fe atom. The Fe–Fe distances of **8** and **9** are somewhat shorter than those in the structures of H_2-uptake enzyme from DdHase (*Desulfovibrio desulfuricans*) and H_2-evolving enzyme from CpHase (*Clostridium pasteurianum*) (ca. 2.6 Å) [1,6,7], but still in good agreement with the structural data of Fe–Fe bonds (2.49–2.51 Å) found in other diiron azadithiolates [12,13,24]. For complex **8**, the twisted flexible chain of ethylenediamine gives the *p*-tosyl group a different orientation from that of phenyl and benzyl-substituents of the ADT-bridged diiron complexes [19,20]. By viewing N(1)–C(9)–C(10)–N(2), the torsion angle 65.9° accounts for the gauche conformation with rotation around the central C9–C10 bond. This indicates that steric factors are important for the rotational energy barriers. N(1) has an approximately tetrahedral shape, with three bonds and a lone-pair. The lone-pair lies directed towards the adjacent carbonyl ligand, i.e. C(1) in **8**. The conformation about N(1) is well described by the S(2)–C(8)–N(1)–C(9) torsion angle 145.9°. This *trans* conformation has the lone-pair pointing towards C(1). In the solid state, the nonbonding C···N distance between the ADT nitrogen atom and the nearest carbonyl carbon atom is almost consistent with the benzyl-substituted analogue (3.01 and 3.02 Å, respectively), which is significantly shorter than that of phenyl-substituted analogues (3.5 Å) [19,25]. Actually, the environment of N(1) is similar to that of benzyl-substituted ADT-bridged diiron complexes. Whereas in the gauche arrangement, the lone-pair is directed away from that carbonyl group, as found in compound **9** which is consistent with the usual phenyl-substituted analogues (Table 2). The torsion angle of S(2)–C(8)–N(1)–C(9) is about 82.0°. The nonbonding C···N distance from the nearest carbonyl carbon atom to the ADT nitrogen atom

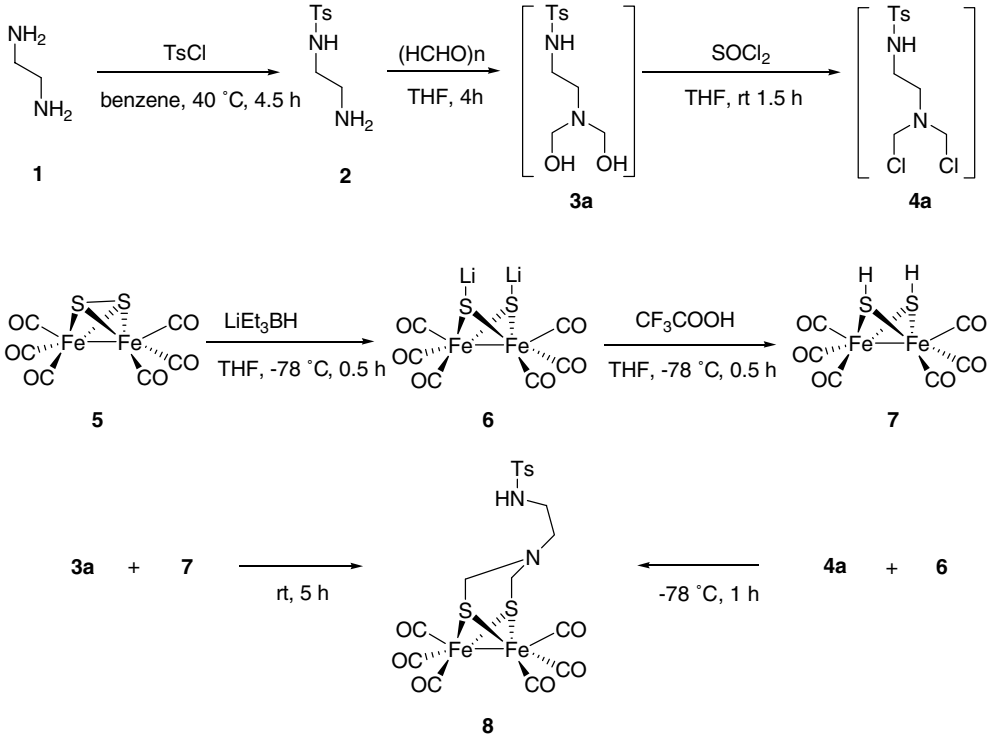

Scheme 1. The synthetic procedure of complex **8**.

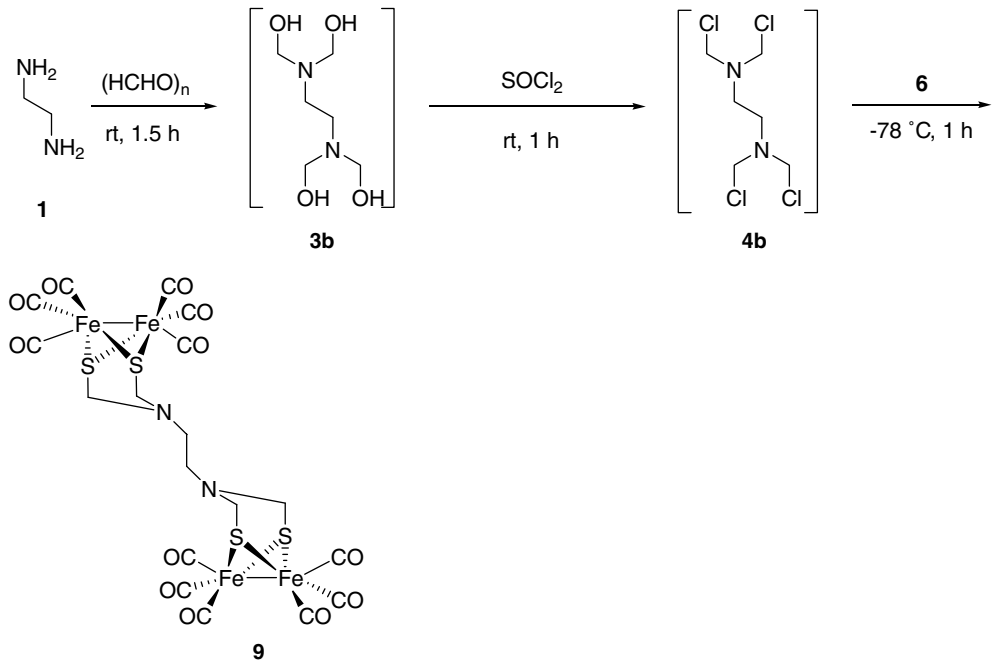

Scheme 2. The synthetic procedure of complex **9**.

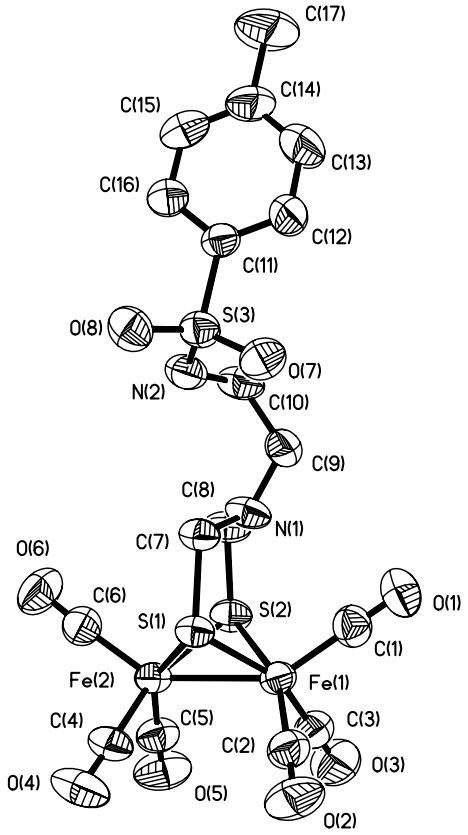

Fig. 2. ORTEP (ellipsoids at 30% probability) diagram of **8**.

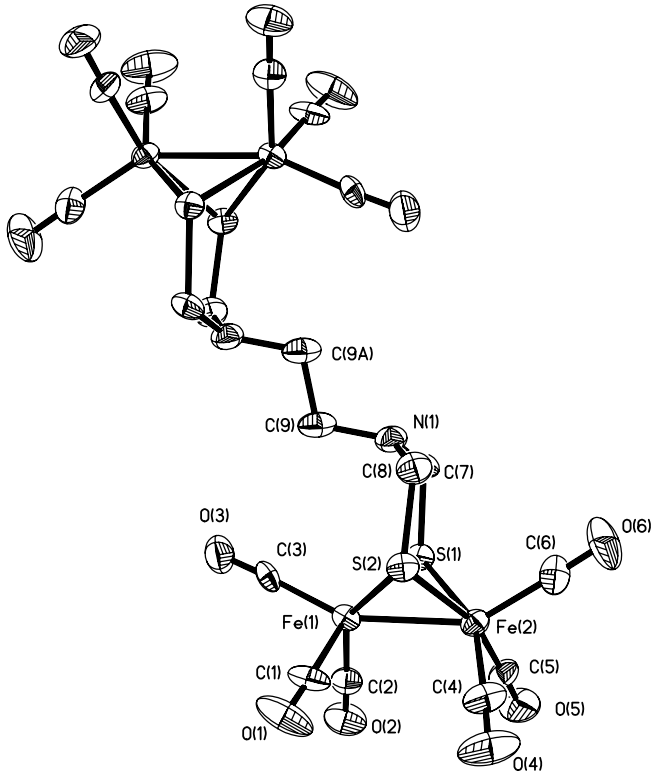

Fig. 3. ORTEP (ellipsoids at 30% probability) diagram of **9**.

(3.69 Å) is even longer than that of the phenyl-substituted analogues.

For complex **9**, it has an absolutely symmetric structure of C_{2v}. Complex **9** has a crystallographically symmetrical structure, with an inversion centre at the mid-point of the C(9)–C(9A) bond. When observing N(1)–C(9)–C(9A)–N(1A), this chain does not twist like that of **8**, rather it takes the zig-zag form.

Table 2
Selected crystal data among different kinds of N atoms in ADT diiron complexes

Compound	Torsion angle (°) (S–C–N–C)[a]	C···N distance[a] (Å)	Bond angle (°) (–C–N–C–)[b]
8	145.9/147.3	3.01	115.0
9	82.0/83.2	3.69	115.6
[20]	159.80/155.83	3.02	114.0
[19]	89.54/96.78	3.50	113.0

[a] From the nearest carbonyl carbon atom to the ADT nitrogen atom.
[b] ADT nitrogen atom [19,20].

Table 3
Selected bond lengths (Å) and angles (°) for complex **8**

Fe(1)–C(2)	1.778(10)	Fe(2)–C(5)	1.802(12)
Fe(1)–C(3)	1.798(12)	Fe(2)–C(4)	1.796(11)
Fe(1)–C(1)	1.816(12)	Fe(2)–C(6)	1.801(12)
Fe(1)–S(1)	2.249(3)	Fe(2)–S(2)	2.250(3)
Fe(1)–S(2)	2.250(3)	Fe(2)–S(1)	2.245(3)
Fe(1)–Fe(2)	2.5152(18)		
C(2)–Fe(1)–C(3)	89.7(5)	C(4)–Fe(2)–C(6)	100.0(5)
C(2)–Fe(1)–S(1)	88.5(3)	C(4)–Fe(2)–S(1)	88.6(3)
C(3)–Fe(1)–S(1)	158.4(3)	C(6)–Fe(2)–S(1)	104.7(3)
C(1)–Fe(1)–S(1)	102.8(4)	C(5)–Fe(2)–S(1)	152.0(3)
C(2)–Fe(1)–S(2)	158.6(3)	C(4)–Fe(2)–S(2)	162.7(3)
C(3)–Fe(1)–S(2)	88.3(4)	C(6)–Fe(2)–S(2)	97.2(3)
C(1)–Fe(1)–S(2)	100.3(4)	C(5)–Fe(2)–S(2)	87.8(4)
S(1)–Fe(1)–S(2)	85.52(10)	S(1)–Fe(2)–S(2)	85.60(10)

Table 4
Hydrogen bonds for complex **8** [Å and °].

D–H···A	d(D–H)	d(H···A)	d(D···A)	∠(DHA)
N(2)–H(2A)···O(8)[a]	0.86	2.13	2.982(10)	172.8

[a] Symmetry transformations used to generate equivalent atoms: $-x$, $-y+1$, $-z$.

Table 5
Selected bond lengths (Å) and angles (°) for complex **9**[a]

Fe(1)–C(2)	1.801(10)	Fe(2)–C(5)	1.797(9)
Fe(1)–C(3)	1.800(10)	Fe(2)–C(4)	1.802(10)
Fe(1)–C(1)	1.807(10)	Fe(2)–C(6)	1.803(11)
Fe(1)–S(1)	2.264(2)	Fe(2)–S(2)	2.262(2)
Fe(1)–S(2)	2.282(2)	Fe(2)–S(1)	2.264(2)
Fe(1)–Fe(2)	2.5062(17)		
C(2)–Fe(1)–C(3)	97.7(4)	C(5)–Fe(2)–C(4)	91.1(4)
C(2)–Fe(1)–C(1)	92.9(4)	C(5)–Fe(2)–C(6)	98.3(4)
C(3)–Fe(1)–C(1)	96.8(5)	C(4)–Fe(2)–C(6)	101.7(5)
C(2)–Fe(1)–S(1)	89.5(3)	C(5)–Fe(2)–S(2)	162.0(3)
C(3)–Fe(1)–S(1)	101.2(3)	C(4)–Fe(2)–S(2)	89.1(4)
C(1)–Fe(1)–S(1)	161.4(4)	C(6)–Fe(2)–S(2)	99.3(3)
C(2)–Fe(1)–S(2)	147.8(3)	C(5)–Fe(2)–S(1)	88.0(3)
C(3)–Fe(1)–S(2)	114.4(3)	C(4)–Fe(2)–S(1)	155.2(4)
C(1)–Fe(1)–S(2)	84.3(3)	C(6)–Fe(2)–S(1)	103.0(4)
S(1)–Fe(1)–S(2)	83.90(9)	S(2)–Fe(2)–S(1)	84.34(8)

[a] A: $-x+1$, $-y$, $-z+1$.

3.3. Protonation of model complexes

The protonation reactions of compounds **8** and **9** to form $\mathbf{8H}^+$ and $\mathbf{9H}_2^{2+}$ were followed by changes in the ^{1}H NMR spectra upon addition of triflic acid to CD_3CN solution of the respective complex. In the case of complex **8**, no peaks at $\delta < 0$ exist in the ^{1}H NMR, showing that the protonation occurred on the N atom rather than to form μ-H complex. Most of the peaks are generally shifted to lower magnetic field than those of **8**. However, the methylene protons in proximity of the ADT nitrogen (–NCH_2S–) were split from 3.43 ppm (singlet) into 3.06 ppm (triplet) and 4.29 ppm (doublet) in a ratio of 1:1. The protons (–NCH_2CH_2NTs) were shifted from 2.83 ppm (doublet) to the region 3.23–3.29 ppm (multiplet). The carbonyl frequencies in the IR spectrum of $\mathbf{8H}^+$ were also shifted 10–18 cm^{-1} to higher in frequency energy relative to those of **8**, which was consistent with the observations made during the protonation of a related complex [12]. Protonation of **8** was accompanied by a color change from orange to yellow. The UV absorption maximum was shifted from 328 to 333 nm, and an isosbestic point was preserved at 320 nm, which indicated the formation of a single protonation product at different concentrations [20]. The changes in ^{1}HNMR, IR and UV absorptions of **9** were similar to those of **8** during the protonation. The ^{1}H NMR and the kinetic UV absorption are shown in Figs. 4, 5 and 6, 7, respectively.

On addition of triflic acid, the methylene protons of **9** (–NCH_2S–) in the ^{1}H NMR were changed from 3.54 ppm (singlet) to 3.21 ppm (triplet) and 4.08 ppm (doublet) in a ratio of 1:1. The peak for the chain protons (–NCH_2CH_2NH–) was shifted from 2.64 to 3.38 ppm. Independent of whether an equivalent amount or an excess of triflic acid was added, the behavior in the ^{1}H NMR is the same. Mainly due to the limitation of solubility of compound **9**, no stepwise protonation was observed under the conditions in our experiment and the protonation occurred for the two N concomitantly.

3.4. Electrochemistry

The formal potentials for complexes **8** and **9** had been determined by cyclic voltammetry in CH_3CN for the evaluation of their redox properties (Fig. 8). Complex **8** exhibited clearly an irreversible oxidation couple at 0.64 V and a quasi-reversible reduction couple at −1.49 V (versus Ag/$AgNO_3$). Complex **9** exhibited two irreversible oxidation peaks at 0.66 and 0.87 V, respectively, and an irreversible reduction peak at −1.51 V, although the solubility of **9** was poor in CH_3CN. Both the one oxidation peak for **8** and the two oxidation peaks for **9** were assigned to one electron process $Fe^IFe^I/Fe^{II}Fe^I$. The reduction waves observed for **8** and **9** were described as one electron processes Fe^IFe^I/Fe^0Fe^I. This set of data followed the general trend discussed for that of PDT and EDT (SCH_2CH_2S)

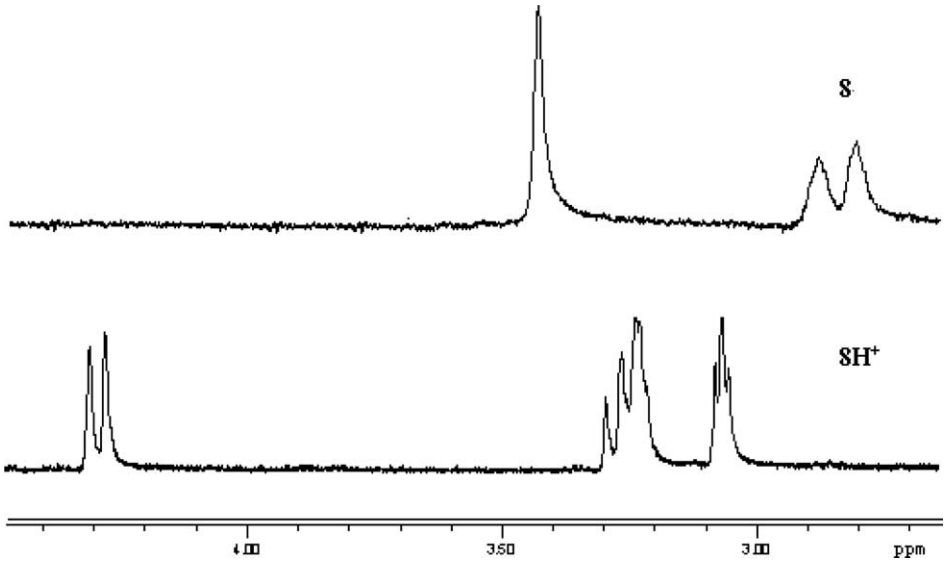

Fig. 4. The ^{1}HNMR spectra of (–NCH_2S–) and (–NCH_2CH_2NH–) for complexes **8** and **8H**$^+$.

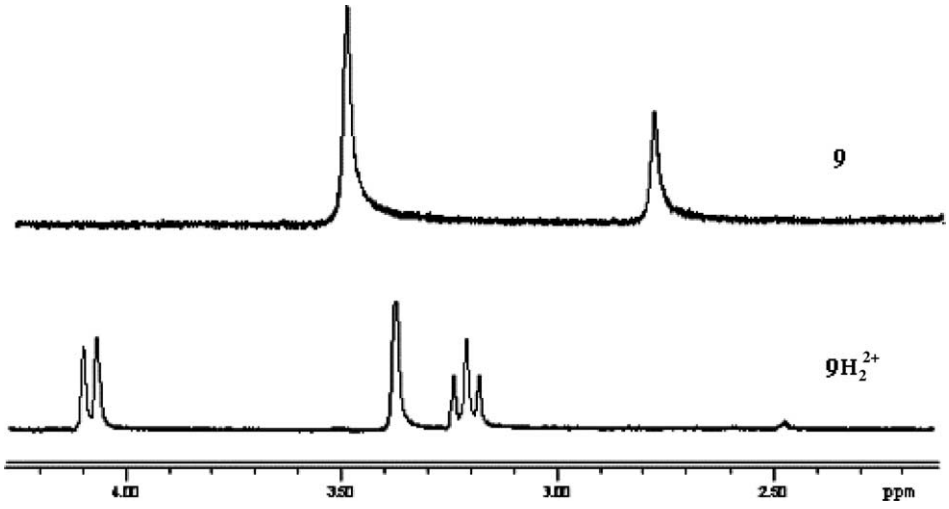

Fig. 5. The ^{1}H NMR spectra of (–NCH_2S–) and (–NCH_2CH_2NH–) for complexes **9** and **9H**$_2^{2+}$.

bridged diiron complexes [26–31] and especially that of [(μ-$SCH_2)_2$N(4-XC_6H_4)]$Fe_2(CO)_6$ (X = NO_2 or NH_2) [19] (Table 6). Compared to the (μ-PDT)$Fe_2(CO)_6$, the oxidation potential of **8** for $Fe^IFe^I/Fe^{II}Fe^I$ was less positive; while for **9**, one of the oxidation potentials for Fe^IFe^I/Fe^{II}-Fe^I was less positive, the other was a little more positive. There seemed to be a mutual effect between the two Fe_2S_2 structures. We could clearly see that complexes **8** and **9** would be easier to reduce than (μ-PDT)$Fe_2(CO)_6$ and more difficult to reduce than [(μ-$SCH_2)_2$N(4-XC_6H_4)]$Fe_2(CO)_6$ (X = NO_2 or NH_2). The difference of inductive effects between aliphatic and aromatic chains could explain for the varying electron density of iron cores. Complex **8** was a little more readily to reduce than **9**, perhaps because of a relatively stronger inductive effect of TsNH.

Proton reduction catalyzed by **8** and **9** was studied by cyclic voltammograms in the presence of a strong acid, CF_3SO_3H (0–10, 30 mM,) in CH_3CN (Fig. 9). The first reduction peak appeared at about −1.18 V both in **8** and **9** when 2.0 mM CF_3SO_3H was added; at the same time the two oxidation peaks for **9** at 0.66 and 0.88 V disappeared, and a new oxidation wave at 0.75 V appeared. The good solubility of **9H**$_2^{2+}$ in CH_3CN made the two Fe_2S_2 subunits equal, giving just a single oxidation peak. The current intensities of all reduction peaks grew further with the increase of the acid concentration and the peaks gradually moved to more negative potential. A sharp increase of current intensity occurred, which reached ca. 900 μA for **8** and **9**, almost 10 times more than that of [(μ-$SCH_2)_2$N(4-$NO_2C_6H_4$)]$Fe_2(CO)_6$ when the concentration of acid increased to 30 mM

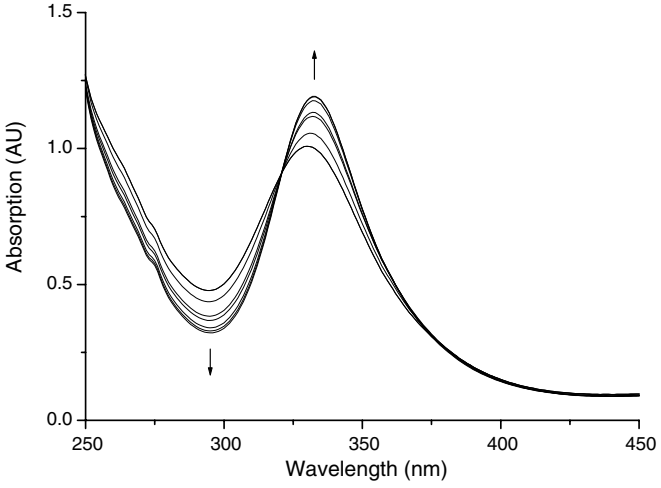

Fig. 6. UV/Vis spectra of **8** (1 mM) in CH_3CN. Arrows indicate spectra changes upon addition of increasing amounts of acid (concentrations of perchloric acid: from 1 to 7 mM).

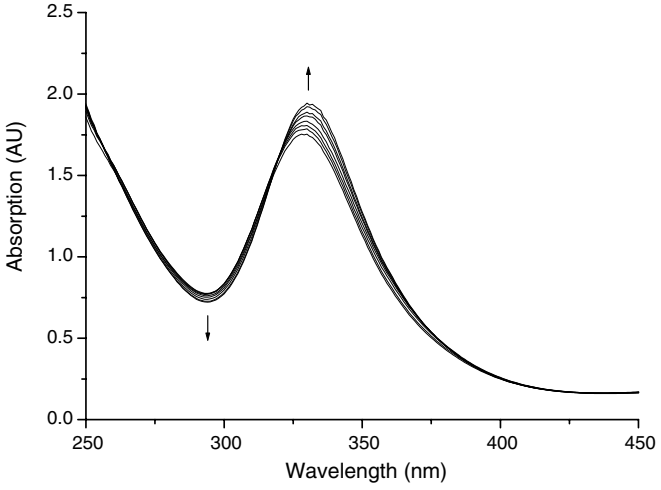

Fig. 7. UV/Vis spectra of **9** (1 mM) in CH_3CN. Arrows indicate spectra changes upon addition of increasing amounts of acid (concentrations of perchloric acid: from 1 to 7 mM).

[19]. It seems that the spacial factors and electron density differences of aliphatic and aromatic chain caused the difference of protonation efficiency. Of course, all of these features were indicative of catalytic proton reduction. Without the diiron complex, reduction of protons at the carbon electrode was slow at the potential of the reduction peak. In the case of both **8** and **9**, we could observe bubbles get out from the surface of the glassy carbon disc when enough CF_3SO_3H was added during the CV measurement. These bubbles were molecular hydrogen which had been identified by GC as before with a similar catalyst [20]. Based on the data of structure and electrochemistry, we propose the catalytic cycle mechanism as the CECE (chemical–electrochemical–chemical–electrochemical) process [19,20].

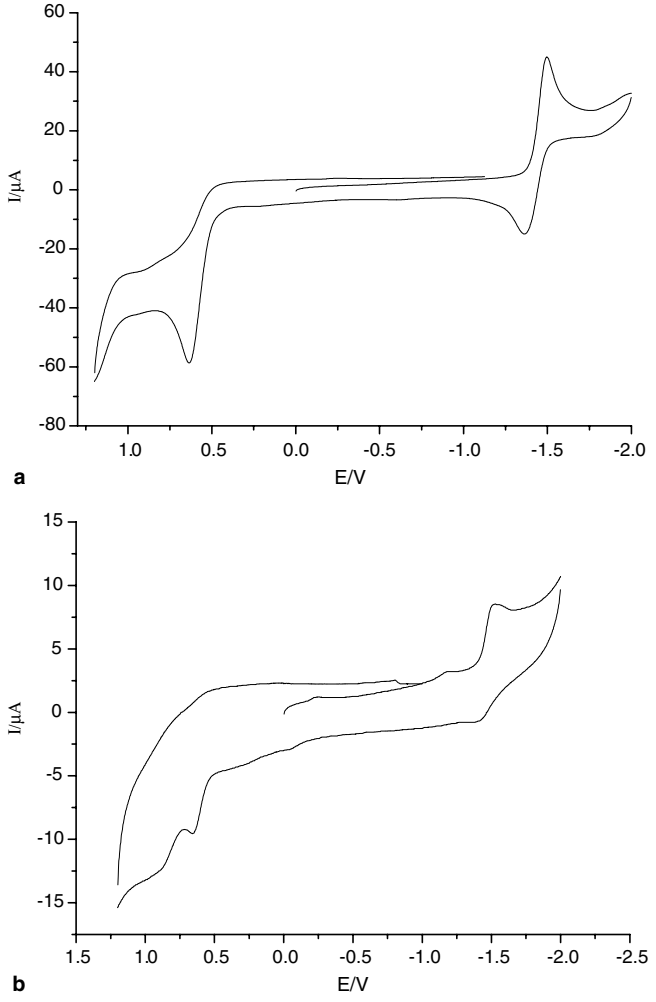

Fig. 8. Cyclic voltammograms of **8** (a) and **9** (b), 2.0 mM in 0.05 M *n*-Bu_4NPF_6/CH_3CN at a scan rate of 100 mV/s.

Table 6
Electrochemical data of complexes **8** and **9**[a]

Compound	E^{oxl}_{pirr} (*V*) $Fe_2(^{I,I})/(^{II,I})$	E_{pc}, E_{pa} (V) $Fe_2(^{I,I})/(^{0,I})$	E_{pc}, E_{pa} (V) $Fe_2(^{0,I})/(^{0,0})$
8	+0.64	−1.49 −1.36	
9	+0.66; +0.87	−1.51 −1.42	
$[(\mu\text{-}SCH_2)_2N\text{-}(4\text{-}NO_2C_6H_4)]Fe_2(CO)_6$	+0.78	−1.34 −1.28	−1.71 −1.63
$[(\mu\text{-}SCH_2)_2N\text{-}(4\text{-}NH_2C_6H_4)]Fe_2(CO)_6$	+0.80	−1.48 −1.23	
$(\mu\text{-PDT})Fe_2(CO)_6$	+0.84	−1.57 −1.47	$E_{pc} = -2.11$

[a] All potentials in Table 4 are vs. Ag/Ag^+ (0.01 M $AgNO_3$ in CH_3CN).

4. Conclusion

Two amino-substituted diiron azadithiolate complexes $[N(CH_2CH_2NHTs)(\mu\text{-}SCH_2)_2]Fe_2(CO)_6$ (**8**) and $[(\mu\text{-}SCH_2)_2Fe_2(CO)_6NCH_2CH_2N(\mu\text{-}SCH_2)_2]Fe_2(CO)_6$ (**9**) have

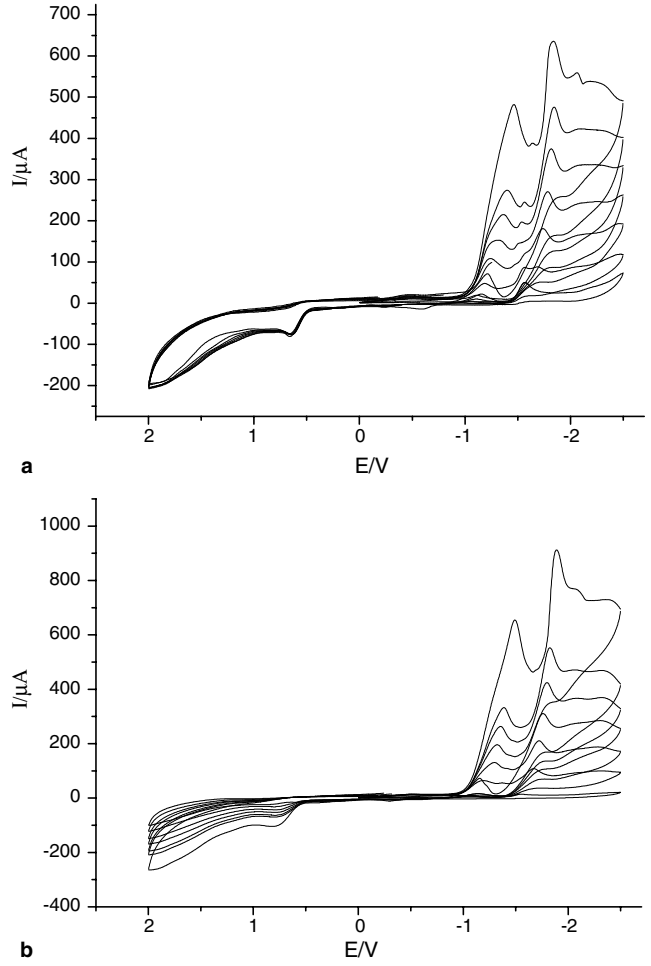

Fig. 9. Cyclic voltammograms of **8** (a) and **9** (b) (2.0 mM) with CF_3SO_3H (0, 2, 4, 6, 8, 10, 30 mM).

been synthesized and characterized by ^1H NMR, IR, UV–Vis and X-ray crystallography. Protonation of complexes **8** and **9** occurred on the bridged-N and no evidence for the formation of Fe–Fe μ-H species was observed. The reduction potentials of **8** and **9** were a little more negative than *N*-phenyl substituted complexes, but more positive than (μ-PDT)$Fe_2(CO)_6$. This may indicate that the aliphatic nitrogen atom of the bridge was different from the aromatic nitrogen in facilitating the formation of protonated iron sulfur intermediates. In this aspect, **8** and **9** showed a better capability of catalyzing electrochemical reduction of protons to molecular hydrogen.

5. Supplementary material

Crystallographic data for the structural analysis have been deposited with the Cambridge Crystallographic Data Center, CCDC-244317 for complex **8** and CCDC-253219 for complex **9**. These data can be obtained free of charge at www.ccdc.cam.ac.uk/conts/retrieving.html or from the Cambridge Crystallographic Data Center, 12 Union Road, Cambridge CB2 1EZ, UK (fax: +441223/336-033 or e-mail: deposit@ccdc.cam.ac.uk).

Acknowledgements

We are grateful to the Ministry of Science and Technology of China and the Chinese National Natural Science Foundation (Grant No. 20128005) for financial support of this work. We are also grateful to the Swedish Energy Agency and the Swedish Research Council for support. We thank Ms. Rong Zhang for the HRMS measurements.

References

[1] J.W. Peters, W.N. Lanzilotta, B.J. Lemon, L.C. Seefeldt, Science 282 (1998) 1853.
[2] R. Cammack, Nature 397 (1999) 214.
[3] D.J. Evans, C.J. Pickett, Chem. Soc. Rev. 32 (2003) 268.
[4] M.Y. Darensbourg, E.J. Lyon, J.J. Smee, Coord. Chem. Rev. 206-207 (2000) 533.
[5] M. Frey, Chem. Bio. Chem. 3 (2002) 153.
[6] Y. Nicolet, C. Piras, P. Legrand, C.E. Hatchikian, J.C. Fontecilla-Camps, Structure 7 (1999) 13.
[7] Y. Nicolet, A.L. Lacey, X. Vernéde, V.M. Fernandez, E.C. Hatchikian, J.C. Fontecilla-Camps, J. Am. Chem. Soc. 123 (2001) 1596.
[8] H.J. Fan, M.B. Hall, J. Am. Chem. Soc. 123 (2001) 3828.
[9] M. Schmidt, S.M. Contakes, T.B. Rauchfuss, J. Am. Chem. Soc. 121 (1999) 9736.
[10] E.J. Lyon, I.P. Georgakaki, J.H. Reibenspies, M.Y. Darensbourg, Angew. Chem., Int. Ed. 38 (1999) 3178.
[11] J.D. Lawrence, H. Li, T.B. Rauchfuss, Chem. Commun. (2001) 1482.
[12] J.D. Lawrence, H. Li, T.B. Rauchfuss, M. Bénard, M. Rohmer, Angew. Chem., Int. Ed. 40 (2001) 1768.
[13] H. Li, T.B. Rauchfuss, J. Am. Chem. Soc. 124 (2002) 726.
[14] S.J. George, Z. Cui, M. Razavet, C.J. Pickett, Chem. Eur. J. 8 (2002) 4037.
[15] W. Liaw, W. Tsai, H. Gau, C. Lee, S. Chou, W. Chen, G. Lee, Inorg. Chem. 42 (2003) 2783.
[16] A.L. Cloiree, S.P. Best, S. Borg, S.C. Davies, D.J. Evans, D.L. Hughes, C.J. Pickett, Chem. Commun. (1999) 2285.
[17] E.J. Lyon, I.P. Georgakaki, J.H. Reibenspies, M.Y. Darensbourg, J. Am. Chem. Soc. 123 (2001) 3268.
[18] J.D. Lawrence, T.B. Rauchfuss, S.R. Wilson, Inorg. Chem. 41 (2002) 6193.
[19] T. Liu, M. Wang, Z. Shi, H. Cui, W. Dong, J. Chen, B. Åkermark, L. Sun, Chem. Eur. J. 10 (2004) 4474.
[20] S. Ott, M. Kritikos, B. Åkermark, L. Sun, R. Lomoth, Angew. Chem., Int. Ed. 43 (2004) 1006.
[21] S. Salyi, M. Kritikos, B. Åkermark, L. Sun, Chem. Eur. J. 9 (2003) 557.
[22] H. Wolpher, M. Borgström, L. Hammarström, J. Bergquist, V. Sundström, S. Styring, L. Sun, B. Åkermark, Inorg. Chem. Commun. 6 (2003) 989.
[23] (a) D. Seyferth, R.S. Henderson, L. Song, Organometallics 1 (1982) 125;
(b) D. Seyferth, R.S. Henderson, J. Organomet. Chem. 218 (1981) C34.
[24] S. Ott, M. Borgström, M. Kritikos, R. Lomoth, J. Bergquist, B. Åkermark, L. Hammarström, L. Sun, Inorg. Chem. 43 (2004) 4683.
[25] S. Ott, M. Kritikos, B. Åkermark, L. Sun, Angew. Chem., Int. Ed. 42 (2003) 3285.
[26] F. Gloaguen, J.D. Lawrence, T.B. Rauchfuss, J. Am. Chem. Soc. 123 (2001) 9476.
[27] F. Gloaguen, J.D. Lawrence, M. Schmidt, S.R. Wilson, T.B. Rauchfuss, J. Am. Chem. Soc. 123 (2001) 12518.

[28] F. Gloaguen, J.D. Lawrence, T.B. Rauchfuss, M. Bénard, M. Rohmer, Inorg. Chem. 41 (2002) 6573.
[29] D. Chong, I.P. Georgakaki, R. Mejia-Rodriguez, J. Sanabria-Chinchilla, M.P. Soriaga, M.Y. Darensbourg, J. Chem. Soc., Dalton Trans. (2003) 4158.
[30] W. Liaw, N. Lee, C. Chen, C. Lee, G. Lee, S. Peng, J. Am. Chem. Soc. 122 (2000) 488.
[31] M. Razavet, S.C. Davies, D.L. Hughes, J.E. Barclay, D.J. Evans, S.A. Fairhurst, X. Liu, C.J. Pickett, J. Chem. Soc., Dalton Trans. (2003) 586.